Heliyon 10 (2024) e27308

Contents lists available at ScienceDirect

Heliyon

journal homepage: www.cell.com/heliyon

Research article

Structural performance of detachable precast concrete column-column joint

H. Zhan [a], M. Ye [a], J. Jiang [b,*], Y. Gao [c], C.W. Zheng [a], S.C. Duan [a]

[a] Research Centre of Wind Engineering and Engineering Vibration, Guangzhou University, Guangzhou, 510006, China
[b] Department of Civil Engineering and Smart Cities, Shantou University, 515063, China
[c] School of Marine Engineering Equipment, Zhejiang Ocean University, 316022, China

ARTICLE INFO

Keywords:
Precast concrete column-column joints
Seismic performance
Hysteresis curve
Skeleton curve

ABSTRACT

A novel type of detachable precast concrete column-column joint (DPC) is proposed in this study to solve the problems in current column-column dry connections including complex load path, uncertainty of structural stiffness of beam-column joints and inconvenience for disassembly. The dry connection technology is applied by composing of steel plate and concrete. Finite element models of DPC were created to study its structural performance including hysteresis curve, skeleton curve, ductility, and energy dissipation capacity. The benchmark models are firstly established and validated against the test data and after that a small-scale parametric study is prepared. The effect of axial pressure ratio and eccentricity distance size on the seismic performance of DPC was studied. Results indict that the optimal value of axial pressure ratio ranges from 0.5 to 0.7. With increase of the axial pressure ratio, the ductility coefficient shows a decreasing trend in general. The eccentricity has little effect on the energy dissipation capacity of the joint.

1. Introduction

Precast concrete column-column joint has a clear advantage in construction cost and energy consumption compared with the traditional construction of reinforced concrete structure [1,2]. However, the safety, structural performance and workability of the joint should be as reliable as cast-in-place concrete construction. The available precast concrete joint usually uses welding [3–5], prestressing [6], laminated beams [7,8] and profiled concrete [9,10] to connect different prefabricated members for the advantages of fast construction and less on-site casting operations. In addition, the seismic performance of traditional connection technology is unsatisfactory [11]. At present, there are two popular ways (dry connection and wet connection) available for precast concrete structure. Compared with wet connection structures, dry connection structures are easier for detachable operation. Hu et al. [12] proposed a dry joint based on precast concrete columns with flange plate connections and showed that columns with flange plate connection have similar seismic performance as conventional cast-in-place columns. Yamashita [13] et al. conducted an experimental study and finite element study of precast concrete columns and a shaking table test study of natural seismic waves on the test members of concrete columns. Shi et al. [14] proposed a fully precast steel frame connection consisting of cold-formed box columns, hot-rolled I-beams, end plate nodes, flexible supports and bolted precast plates, and conducted an experimental study of the structure consisting of this node connection and obtained the conclusion that the node has good cyclic performance, high horizontal bearing capacity and good

* Corresponding author.
E-mail address: jian0048@e.ntu.edu.sg (J. Jiang).

https://doi.org/10.1016/j.heliyon.2024.e27308
Received 1 March 2023; Received in revised form 22 February 2024; Accepted 27 February 2024
Available online 5 March 2024

ductility.

Kulkarni et al. [15] proposed a steel-concrete connection and studied the key parameters affecting the performance of the connection. Jiang et al. [16] proposed a recoverable steel beam-column connection and found that reasonable design of the connection parameters can make the beam-column exhibit good bearing capacity, seismic performance, and ductility. Nzabonimpa et al. [17–22] conducted an experimental and nonlinear numerical study of mechanical connections between reinforced concrete laminated plates and concrete laminated slabs for transferring axial loads and bending moments and proposed a hybrid mechanical joint with laminated metal plates instead of the conventional grouted sleeve connection for shaped columns. Wei et al. [23] proposed a new type of assembled monolithic column with connection treatment in the form of outer steel plates welded with transverse reinforcement and investigated its seismic performance. Zhang et al. [24] proposed an improved assembled column joint with multiple slot connections. Hua et al. [25–27] proposed a new beam-column bolt-connection with plastically controllable hinges. Compared with frame connected with the cast-in-place joints, the frame connected with the new joints can improve the energy dissipation capacity and ductility. Al-Rousan [28–30] proposed to use carbon fiber and fiber-reinforced polymers to strengthen the connection for seismic performance of beam-column joints. The comparative analysis on compressive bearing capacity and corresponding strain, hysteretic curve, skeleton curve, ductility, energy dissipation capacity and stiffness degradation show that the ductility and energy dissipation capacity of beam-column joints using fiber-reinforced polymers are significantly improved. Jiang et al. [31–35] experimentally investigated the effect of fabrication technique on the seismic performance of the joint. Gao et al. [36] presents numerical findings of reinforced concrete interior beam-column joints under monotonic antisymmetric load.

In order to solve construction inconvenience of the existing column-column dry connection, this paper proposes a detachable precast concrete column-column joint (DPC) based on rigid connection technology. This joint has the characteristics of detachable and strong integrity. The main innovation of this article is to this DPC as dry connection. The influence of the geometrical design of DPC joint on the seismic performance is discussed and an optimal design scheme for the proposed DPC is given.

In this study, a detachable precast concrete column-column (DPC) joint was proposed with high-strength bolts, web connection plate, upper and lower connection plates, I-beam and studs, as shown in Fig. 1(a) and (b). The core part of DPC is the steel connection. In this part, the role of the cladding plate is to prevent stress concentration at the connection gap and to protect the concrete in contact with the cladding plate from being crushed. Steel studs can improve the performance of the connection of precast concrete beams. High-strength bolts and connecting plates are used to connect two steel I-heads for higher shear bearing capacity. Hence, a smaller number can be used to meet the design requirements of bearing capacity. The fewer number of holes reserved for the bolts on the I-beam connector makes higher integrity of the connecting plate and the I-beam connector. The precast concrete part and the steel connection part are prefabricated as a single unit, and the longitudinal reinforcement inside the concrete is welded to the steel connection, as shown in Fig. 2.

The DPC joint was proposed in this study to solve the problems in current column-column dry connections such as complex load path and inconvenience for disassembly. The dry connection technology is applied by composing of steel plate and concrete. Compared with the existing dry joints, another advantage of the DPC joint is that the design methods in the existing steel structure specifications can be used. Finite element models of DPC were created to study its structural performance including structural ductility and energy dissipation capacity. First, the FE modeling technique was validated by testing data. The seismic performance analysis of detachable precast concrete column-column joints (DPC) was then carried out.

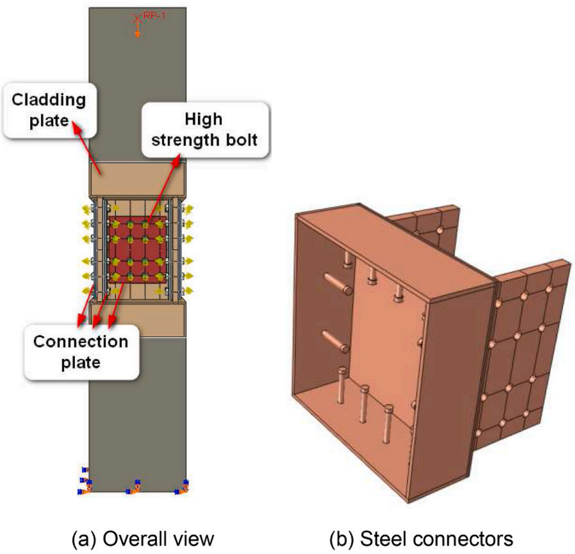

Fig. 1. Detachable precast concrete column-column (DPC) joint.

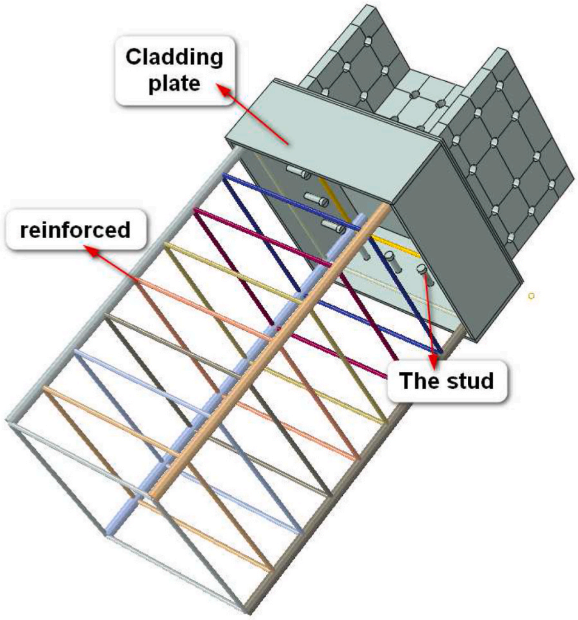

Fig. 2. Details of the DPC joint.

2. Design philosophy of the DPC joint

2.1. The bearing capacity of the cast-in-situ concrete column

To study the structural performance of the DPC joint, a control joint, which is traditionally casted in site, is designed and proposed [37]. The size of cast-in-situ concrete column is 500*500*2500 mm and the protective layer thickness is 30 mm as shown in Fig. 3(a)

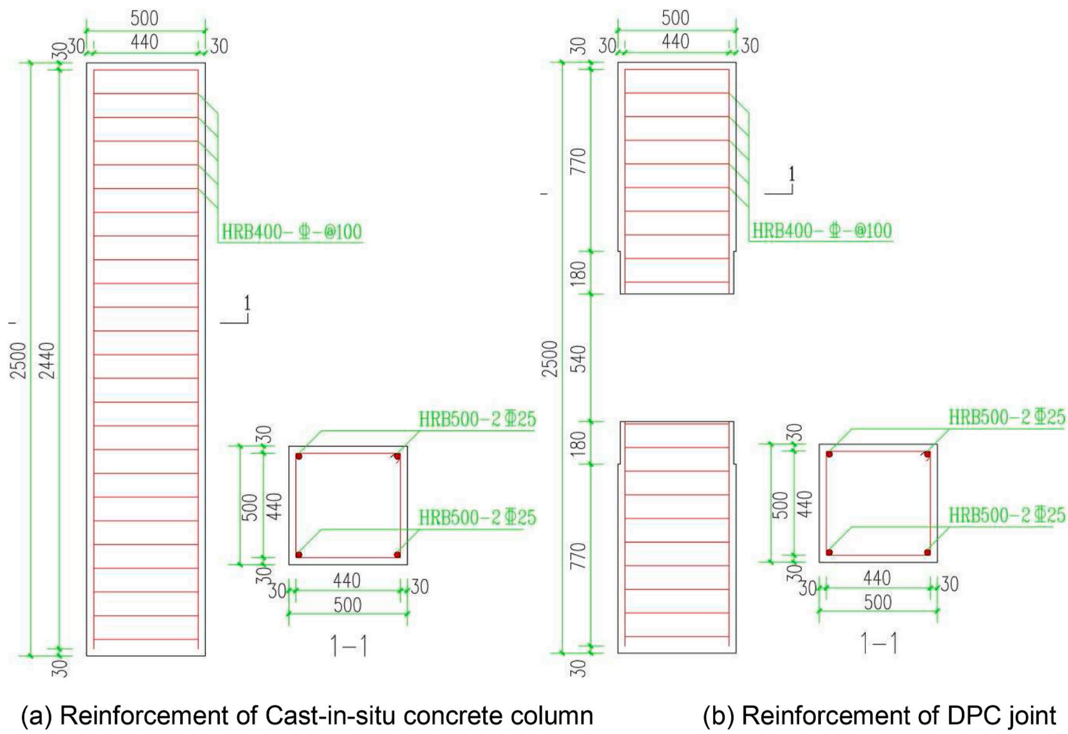

Fig. 3. Geometry design.

and (b). Note that the concrete grade is C40 and the longitudinal reinforcement is 25 mm in diameter and the hoop reinforcement is φ10@100.

First, the ultimate shear bearing capacity of the cast-in-situ concrete column is calculated according to Eqs. (1)–(3) from the Principles of Structural Design of Concrete [38].

$$V_u = \frac{1.75}{\lambda+1} f_t b h_0 + f_{yv} \frac{A_{sv}}{S} h_0 + 0.07N \quad \text{Eq. (1)}$$

$$\lambda = \frac{H_n}{2h_0} \quad \text{Eq. (2)}$$

$$N = 0.3 f_c A \quad \text{Eq. (3)}$$

Where, V_u is the shear bearing capacity of the column; λ is the shear-to-span ratio of the calculated section; f_t is the design value of the concrete shear bearing capacity; b is the section width; h_0 is the effective section height of the column; f_{yv} is the design value of the tensile strength of the hoop reinforcement; A_{sv} is the full cross-sectional area of each limb of the hoop reinforcement in the same section; S is the spacing of the hoop reinforcement along the length of the member; N is the design value of the axial tensile force; H_n is the net height of column; f_c is the design value of axial compression strength of concrete; A is the total cross-sectional area of the column.

Second, the compressive bearing capacity of the cast-in-situ concrete column is calculated according to Eq. (4).

$$N_u = 0.94 \times \left(f_c \mathrm{A} + f_y' A_s'\right) \quad \text{Eq. (4)}$$

Considering the stochastic nature of earthquakes, symmetrical reinforcement was used to make the longitudinal and transverse bearing capacities of the columns the same. Hence, the relative compressive zone height of concrete is calculated by Eq. (5):

$$x = \frac{N_u - f_y' A_s' - f_y A_s}{\alpha_1 f_c b} \quad \text{Eq. (5)}$$

Since the relative compressive zone height $x > \varepsilon_b h_0$, which belongs to the case of small eccentric pressure, recalculate x according to the case of eccentric load (Eq. (6)):

$$\frac{x}{h_0} = \frac{N_u - f_y' A_s' - \frac{0.8}{\varepsilon_b - 0.8} f_y A_s}{\alpha_1 f_c b h_0 - \frac{1}{\varepsilon_b - 0.8} f_y A_s} \quad \text{Eq. (6)}$$

Where, N_u is the compressive bearing capacity of the cast-in-place columns; f_c is the design value of the concrete compressive bearing capacity; A is the cross-sectional area of the member; f_y is the design value of the compressive strength of the reinforcement; A'_s is the cross-sectional area of all longitudinal reinforcement; x is the height of the concrete compressive zone; α_1 is the coefficient of the equivalent rectangular stress diagram of the concrete compressive zone, and takes the value of 1 when the concrete strength is less than C50; b section width; h_0 is the effective height of the concrete; ε_b is the height of the relative boundary compressive zone.

Then, the eccentricity e and the bending bearing capacity M_u of the cast-in-situ concrete column are calculated by the following Eq. (7) and Eq. (8):

$$\mathrm{e} = \frac{\alpha_1 f_c b x \left(h_0 - \frac{x}{2}\right) + f_y' A_s' (h_0 - a')}{N} \quad \text{Eq. (7)}$$

$$M_\mathrm{u} = N_u \times e \quad \text{Eq. (8)}$$

Finally, according to the size and reinforcement of the cast-in-situ concrete column, the compressive , the shear and the bending bearing capacity of the cast-in-situ concrete column are calculated, as Eq. (9):

$$N_\mathrm{u} = 5180\mathrm{kN}, V_\mathrm{u} = 620\mathrm{kN}, M_\mathrm{u} = 245\mathrm{kN}\cdot\mathrm{m} \quad \text{Eq. (9)}$$

2.2. Design of DPC joint

Based on the bending bearing capacity of the cast-in-situ concrete column Eq. (9), the dimension of the I-beam, the connecting plate and the number of high-strength studs are calculated according to design equations in Steel Connection Node Design Manual [39]. The dimension of the studs is determined according to test results [40]. According to the load-bearing capacity calculation result of the cast-in-situ concrete column, the size of the I-beam column can be initially selected as 420 × 440 × 28 × 20. According to Table 8.1.1 of the Steel Design Criteria [41], plastic development factor of the section $\gamma_x = 1.05$, $\gamma_y = 1.2$ is used for strength calculation by substituting the following Eq. (10).

$$\frac{N_u}{A}+\frac{M_u}{\gamma_x W_{ox}^{o}}+\frac{M_u}{\gamma_y W_{oy}^{0}}<f_y \quad \text{Eq. (10)}$$

Note that Q345 is used for I-beam, the connecting plate and 10.9 grade M30 high-strength bolts friction type double shear connection is used for studs. The number of high-strength bolts is determined according to Eq. (11) and Eq. (12):

$$n_{FC}=\left[\frac{A_F}{A}N_u+\frac{M_u}{(H_c-t_{FC})}\right]\Big/N_V^{bH} \quad \text{Eq. (11)}$$

$$n_{WC}=\sqrt{\left(\frac{A_w}{A}N_u\right)^2+{V_u}^2}\Big/N_V^{bH} \quad \text{Eq. (12)}$$

Where, n_{FC} is the number of high strength bolts required for single side flange; n_{WC} is the number of high strength bolts required for single side web; H_c is the height of I-beam; t_{FC} is the thickness of I-beam flange; N_V^{bH} is the design value of shear bearing capacity of high strength bolts, 238.5 for 10.9 grade high strength bolts; B_c is the width of I-beam flange; t_{WC} is the thickness of I-beam web; h_{WC} is the height of I-beam web.

Considering that the I-beam has two directions of strong axis (X direction) and weak axis (Y direction), the stiffness along two directions (X and Y) were calibrated separately in this paper. First, for the X direction, the net section moment of inertia of the I-beam is equal to the I-beam moment of inertia minus the I-beam bolt hole moment of inertia given by Eq. (13). The net section moment of inertia of the I-beam connecting plate is derived from Eq. (14). The net section modulus is obtained from the net section moment of inertia according to Eq. (15) and Eq. (16).

$$I_{nx}^{c}=I_{ox}^{c}-I_{xR}^{c} \quad \text{Eq. (13)}$$

$$I_{nx}^{pl}=I_{ox}^{pl}-I_{xR}^{pl} \quad \text{Eq. (14)}$$

$$W_{nx}^{c}=\frac{I_{nx}^{c}}{H_c/2} \quad \text{Eq. (15)}$$

$$W_{nx}^{pl}=\frac{I_{nx}^{pl}}{H_c/2+h_c/2} \quad \text{Eq. (16)}$$

Where, I_{ox}^{c} is the moment of inertia of I-steel in x direction; I_{xR}^{c} is the moment of inertia of the bolt hole section in the x-direction of the I-beam; I_{nx}^{c} is the net moment of inertia of the I-beam after deducting the bolt holes in the x-direction of the I-beam; I_{ox}^{pl} is the gross section moment of inertia of the I-beam splice joint plate in the x-direction; I_{xR}^{pl} is the moment of inertia of the bolt hole section in the x-direction of the I-beam splice joint plate;I_{nx}^{pl} is the moment of inertia of bolt hole section in the x direction of I-steel splicing connection plate;W_{nx}^{c} is the net section modulus of the I-beam in the x-direction; W_{nx}^{pl} is the net section modulus in the x direction of I-steel splicing connection plate; W_{oy}^{o} is the net section modulus of the I-beam in the y-direction modulus; is the thickness of the outer flange joint plate; H_c is the height of I-steel; h_c is the thickness of the outer connecting plate of the flange.

3. FE modelling analysis

3.1. Material constitutive model

To precisely model the joint behavior under low-reversed cyclic displacement loads, the plastic damage model (PDM) proposed by J. Lee and GL Fenves [42] was used to model the mechanical behavior of concrete structures. In this model, concrete is regarded as an isotropic material, and the reduction of the concrete elastic stiffness can effectively simulate the characteristics of concrete stiffness decreasing with loading and unloading.

The constitutive model of concrete material is provided in the ABAQUS material library. However, the corresponding relationship between concrete compressive stress and plastic compressive strain, concrete tensile stress and cracking tensile strain needs to be manually input for the plastic stage, since the full stress-strain curve of concrete is difficult obtained. In this study, the calculation method of the stress-strain relationship given by the design code for concrete structures [53] (GB50010-2002) is used. The nominal stress-strain curve is obtained from concrete structural design code as shown in Eqs. 17–20.

When $x \le 1$:

$$\alpha_a x+(3-2\alpha_a)x^2+(\alpha_a-2)x^3 \quad \text{Eq. (17)}$$

When $x > 1$:

$$\frac{x}{\alpha_d(x-1)^2+x} \quad \text{Eq. (18)}$$

$$x = \frac{\varepsilon}{\varepsilon_c} \quad \text{Eq. (19)}$$

During modelling process, the real stress and strain need to be input in the PDM model. Eq. (21) and Eq. (22) are used to convert the nominal stress-strain curve into the real nominal stress-strain curve.

$$y = \frac{\sigma}{f_c} \quad \text{Eq. (20)}$$

$$\sigma c = f_c \times y \quad \text{Eq. (21)}$$

$$\varepsilon_c^{in} = \varepsilon_c \times x - \frac{\sigma_c}{E} \quad \text{Eq. (22)}$$

Where, α_a and α_d are the values of the rising and falling segments of the uniaxial compressive stress-strain curves, respectively; σ, ε are the stress and strain of concrete, respectively; f^*_c are the uniaxial compressive strength of concrete; ε_c is the corresponding peak compressive strain of concrete; σ_c is compression stress inputted in the PDM model; ε_c^{in} is the plastic strain to be input in the PDM model; and E is the modulus of elasticity of concrete.

For reinforcement and steel connection, the bilinear elastoplastic model is used. Table 1 and Table 2 gives concrete input parameters. The input parameters of reinforcement are given in Table 3 and the input parameters of steel are given in Table 4.

3.2. Analysis setting

Fig. 4 gives the loading and boundary condition used in modelling. The tangential behaviour of DPC model is based on the friction equation "penalty" by defining a friction coefficient of 0.45, while the normal behaviour is defined as a "hard contact" for pressure overload. The cladding plate and the column at the joints are connected by binding constraints. The four faces of the beams were set as master faces and the inner surfaces of the cladding slabs were set as slave faces; the longitudinal reinforcement and hoop bars were connected to the concrete through built-in areas and the geometric tolerance is set to the ABAQUS default value of 0.05. Table 5 lists the interactions between parts in modelling.

The symmetric modelling technique [43,44] introduced to simplify the modelling process and reduce the degrees of freedom and the computational cost. The steel bars of cast-in-situ joints and DPC joints are simulated by element type T3D2, while the concrete, steel plate and high-strength bolts are simulated by C3D8R.A finer mesh was used in the connection area between prefabricated members and steel connection, as shown in Fig. 5(b). Similar work can be found from Jiang's research group [31,45,46]. The seismic performance of dry-connection technique was experimentally and numerically studied and the modeling technology used was validated by the test data. Mesh sensitivity analysis was also organized that three mesh size of 12 mm, 6 mm and 2 mm were created (Fig. 5). In this study, The mesh sensitivity study results are summarized in Table 6. It is found that the ultimate bearing capacity does not change significantly for different mesh sizes. However, the mesh size gets smaller, the CPU time required for the analysis increases significantly. Hence, the optimal element size is selected to 5 mm and it is used for the following benchmark models and parametric studies.

3.3. Validation of modelling results

An experimental study on the seismic performance of DPC beam-column joints was carried out and the modelling technique and results were validated by test data [31]. The geometrical parameters of the joints can be referred to the literature [31].

Fig. 6 shows the comparison between hysteresis curves from test and modelling. Note that the ultimate bearing capacity of the joint based on modelling is 203.6 kN, while the ultimate bearing capacity of the test joint is 219.2 kN. Hence, there is only a 7.6% difference between the modelling and test results. Hence, a precise result can be obtained by reasonable modelling technique used.

3.4. Study of seismic performance of DPC joint

In order to study the seismic performance of DPC joint, two loading scenarios, cyclic displacement loading and monotonic displacement, were used in this study. The energy dissipation and the ductility of the joints were obtained and analysed.

Table 1
Stress-strain relationship of the concrete under uniaxial compression.

$f_c^*(N/mm^2)$	15	20	25	30	35	40	45	50	55	60
$\varepsilon_c\ (\times 10^{-6})$	1370	1470	1560	1640	1720	1790	1850	1920	1980	2030
α_a	2.21	2.15	2.09	2.03	1.96	1.90	1.84	1.78	1.71	1.65
α_d	0.41	0.74	1.06	1.36	1.65	1.94	2.21	2.48	2.74	3.00
$\varepsilon_u/\ \varepsilon_c$	4.2	3.0	2.6	2.3	2.1	2.0	1.9	1.9	1.8	1.8

Note : ε_u is the compressive strain of concrete when the stress on the descending section of the stress-strain curve is equal to 0.5 f_c^*.

Table 2
Concrete input parameters.

Expansion angle ψ(°)	Eccentricity $\in$	f_{b0}/f_{c0}	K_c	Viscosity parameters μ
30	0.1	1.16	0.667	0.00005

Notes. f_{b0}/f_{c0} is the ratio of biaxial to uniaxial compressive ultimate strength. K_c is the invariant stress ratio.

Table 3
Rebar input parameters.

column stressing bar yield strength (MPa)	column stressing bar yield strength (MPa)	hoop tendon yield strength (MPa)	modulus of elasticity (MPa)	Poisson's ratio
500	500	400	2×10^5	0.3

Table 4
Steel input parameters.

density (kg/mm3)	Modulus of elasticity (MPa)	Poisson's ratio	Yield stress (MPa)	plastic strain
7.85E-009	200000	0.3	345	0

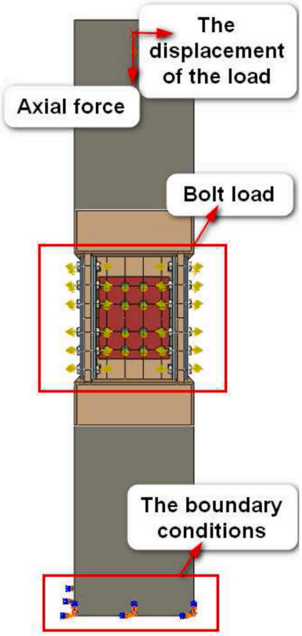

Fig. 4. Loading and boundary condition setting.

3.4.1. Seismic performance analysis under cyclic displacement load

Fig. 7 gives the cyclic displacement loading applied on the top of the column. Fig. 8(a) and (b) show the equivalent cumulated compressive plastic strain of the joints under the applied load. Figs. 9 and 10 show the hysteresis curves and skeleton curves of the cast-in-place joint and the DPC joint. It can be found that the maximum strain occurs mainly at the base of the column. The maximum strain in DPC joint is 0.017 and the maximum strain cast-in-place joint is 0.066. In other word, the maximum strain in DPC joint is reduced by 74.2% compared the cast-in-place joint. This is due to the inclusion of steel structure for DPC joint.

Fig. 9 shows that the hysteresis curves of the DPC joint and cast-in-place joint have the same trend. The hysteresis curves of the two joints almost overlap at the early stage of loading (when the loading displacement is 0–10 mm), indicating that the mechanical properties of the DPC joint at the elastic stage are consistent with those of the conventional cast-in-place column joint. In the middle and late loading stage (the loading displacement is 10–50 mm), both nodes enter the yield stage. The hysteresis curve of DPC node is slightly lower than that of cast-in-place node. Due to the steel structure used at the joints of DPC nodes, the hysteretic curves of DPC

Table 5
Interaction between parts in modelling.

Type of constraint	Part 1	Part 2
Binding constraints	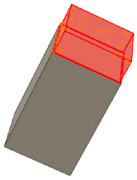 main surface	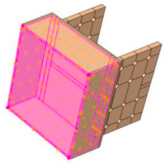 from the surface
built-in area	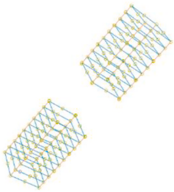 Embedded elements	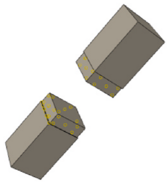 Main elements
Universal contact	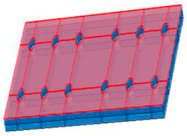 main surface	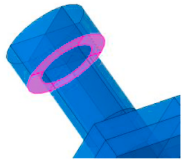 from the surface
coupling	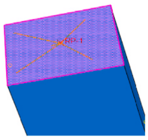 coupling surface	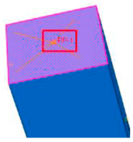 coupling point
built-in area	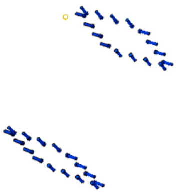 Embedded elements	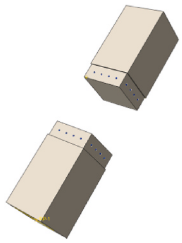 Main elements

nodes are slightly fuller than those of cast-in-place nodes.

To evaluate the deformation capacity from yielding to the maximum bearing capacity for evaluating the seismic performance of the structure, the ductility coefficient can be evaluated according to Eq. (23).

$$\mu_u = \frac{\Delta_u}{\Delta_y} \qquad \text{Eq. (23)}$$

Where μ_u refers to the displacement ductility coefficient; Δ_u refers to the ultimate displacement of the structure in millimetres (mm), which is generally taken as the displacement corresponding to the fall of the member to 0.85 F_{max} after reaching the ultimate load; Δ_y refers to the yield displacement, which is in millimetres (mm).

Table 7 lists the ductility coefficients of the DPC joint and cast-in-place joint. It can be found that the ductility coefficient difference between the two joints is 13.7% while the yield strengths of the two joints are very close. In fact, and the ductility coefficient of DPC joint is greater than that of the cast-in-place joints. A comparison of the joint energy dissipation under cyclic displacement loading is shown in Fig. 11. It can be seen that the energy dissipation capacity trend of the two joints is basically the same. When the loading displacement is 0 mm–10mm, the energy dissipation capacity of the two joint is relatively weak as the energy dissipation capacity of the joints is poor before yielding. When the loading displacement is 10 mm–50mm, the energy dissipation capacity of both joints is

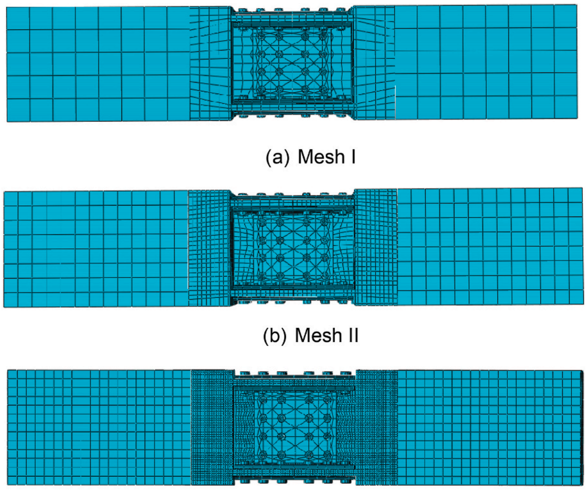

Fig. 5. Mesh sensitivity analysis.

Table 6
The mesh sensitivity analysis.

Mesh	Brick element size (mm)	Cost time (mins)	Ultimate capacity (kN)
Mesh I	12	15	340
Mesh II	6	45	326
Mesh III	2	320	310

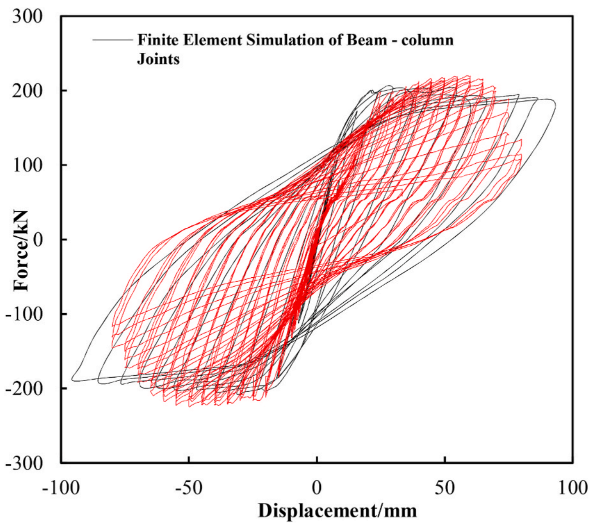

Fig. 6. Validation of the modelling result.

significantly increased. Overall, the energy dissipation capacity of the DPC joint is equivalent to that of cast-in-place joint.

3.4.2. Seismic performance analysis under monotonic displacement load

Fig. 12(a) and Fig. 12(b) show stress contour of the two joints under monotonic displacement load of 0 mm–30mm applied to the top of the column. Fig. 13 shows the force-displacement curves. The stress concentration effect of the cast-in-place joint can be found on the column bottom reinforcement while the stress concentration phenomenon of the DPC joint is mainly located at the high-strength bolts and the column bottom reinforcement.

The initial stiffness is 28.8 kN/mm and 32.2 kN/mm for the cast-in-place joint and DPC joint, respectively. It means DPC joint has a

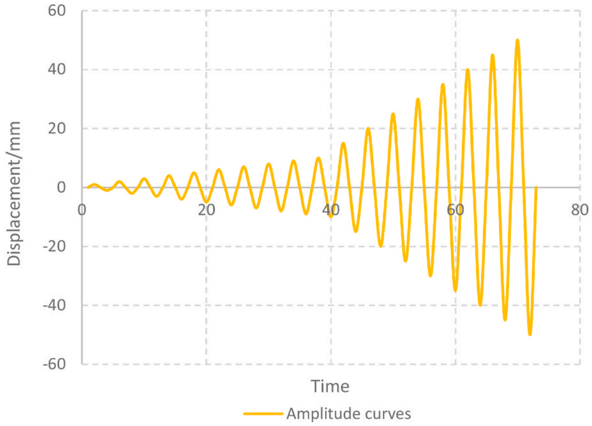

Fig. 7. The cyclic displacement load.

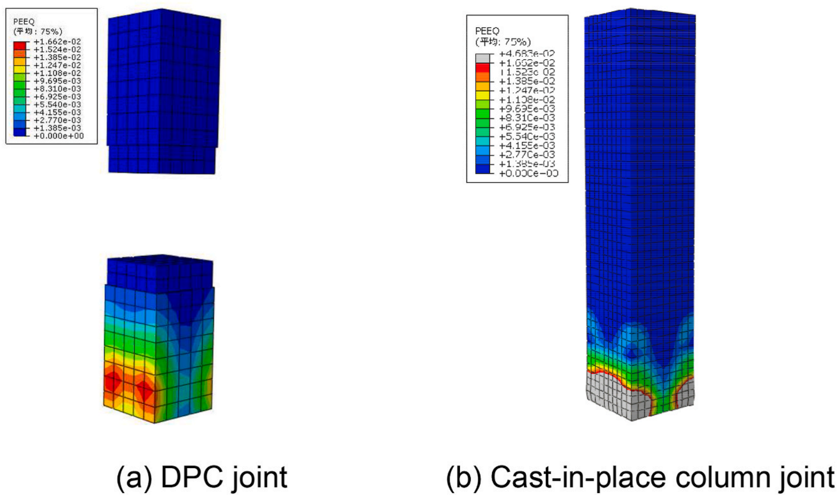

Fig. 8. Concrete strain contour.

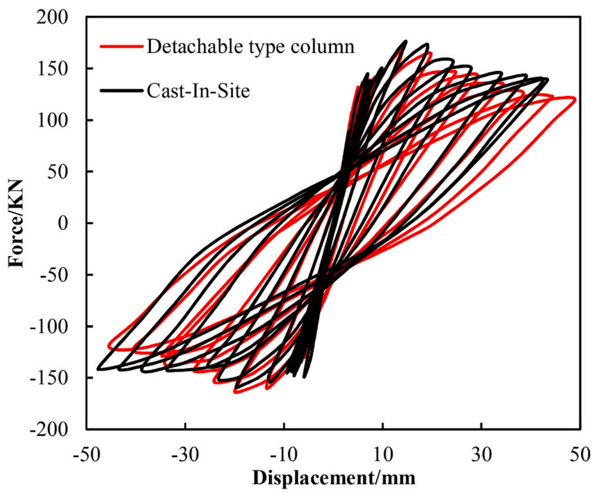

Fig. 9. Hysteresis curve comparison.

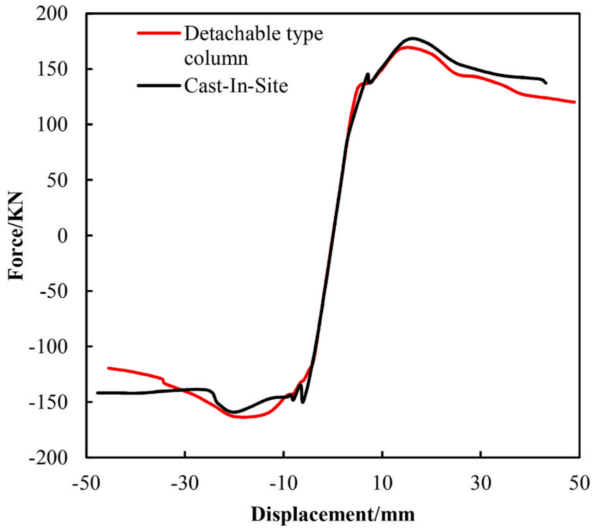

Fig. 10. Skeleton curve comparison.

Table 7
the ductility coefficients of the DPC joint and cast-in-place joint.

models	Loading direction	yield point		Ultimate displacement (mm)	μ_u
		load capacity (kN)	displacement (vector) (mm)		
Cast-in-place nodes	forward	138.13	7.77	43.18	3.93
	negative direction	−137.53	−7.81	−47.68	6.49
Loading and unloading nodes	forward	138.95	7.46	48.96	4.47
	negative direction	−139.07	−7.56	−45.49	4.48

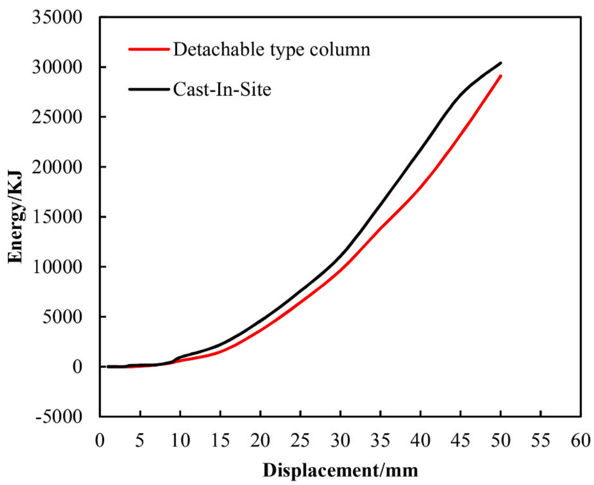

Fig. 11. Energy dissipation capacity comparison.

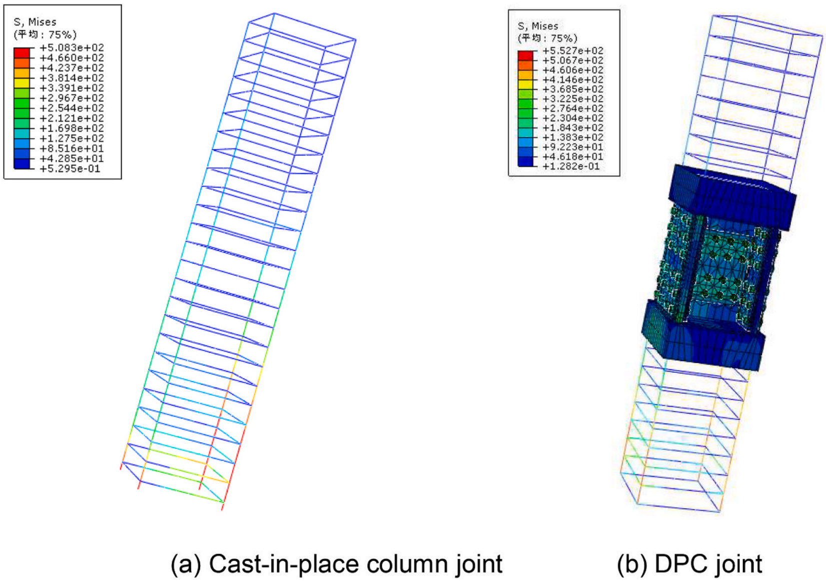

Fig. 12. stress contour of the two joints.

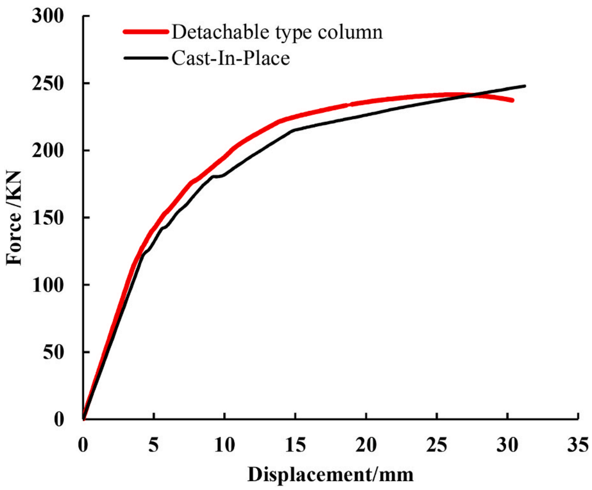

Fig. 13. The force-displacement curve comparison.

11.6% higher initial stiffness and 4.5% higher ultimate bearing capacity than the cast-in-place joint. In summary, it is shown that the seismic performance of the DPC is more or less equivalent to the cast-in-place joint.

4. Parametric study

4.1. Effect of axial pressure ratio

Six FE models with axial pressure ratios of 0.3, 0.4, 0.5, 0.6, 0.7 and 0.8 were created to study the effect of axial pressure ratio on seismic performance of the DPC joint. The hysteresis curve and skeleton curve comparisons are given in Figs. 14 and 15. It can be observed that the axial pressure ratio has important influence on ultimate bearing capacity. However, the axial pressure ratio has no effect on the skeleton curve before yielding. Only on the stage of after yielding, the axial compression ratio has a important impact on ultimate bearing capacity. The energy dissipation energy comparison is shown in Fig. 16. The joint with axial pressure ratio of 0.7 has the best energy dissipation capacity and the joint with axial pressure ratio of 0.4 has the lowest energy dissipation capacity. The energy dissipation capacity of the joint with axial pressure ratio of 0.7 is 16.5% higher than that of the joint with axial pressure ratio of 0.4. The energy dissipation capacity for the joints with axial pressure ratio of 0.5–0.6 is higher than the joint with axial pressure ratio of 0.4 as well.

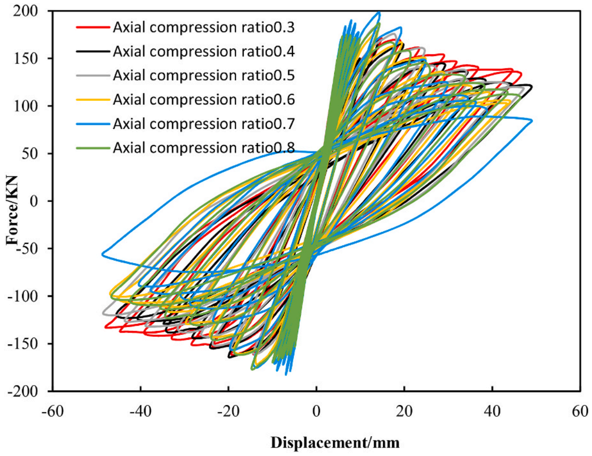

Fig. 14. Hysteresis curve comparison.

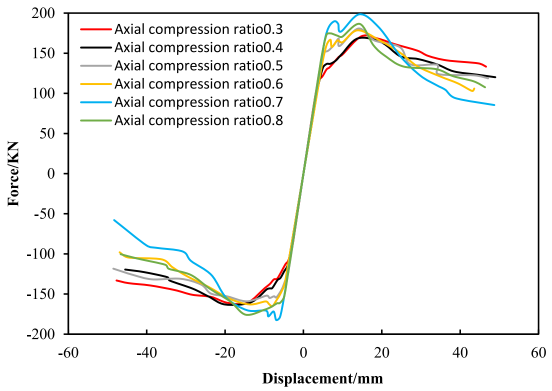

Fig. 15. Skeleton curve comparison.

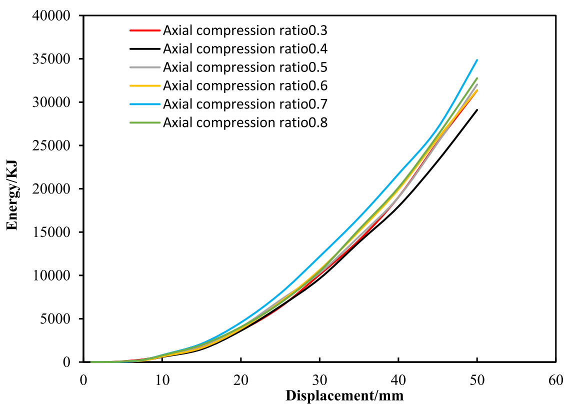

Fig. 16. The energy dissipation energy comparison.

The ductility coefficient comparison is shown in Table 8. With increase of the axial pressure ratio, the ductility coefficient shows a decreasing trend in general. The joint with axial pressure ratio of 0.3 has the largest ductility coefficient. When the axial pressure ratio is between 0.4 and 0.6, the ductility coefficient of the joint changes smoothly.

Table 8
The ductility coefficient comparison.

models	Loading direction	yield point		Ultimate displacement (mm)	μ_u
		load capacity (kN)	displacement (vector) (mm)		
0.3	forward	135.99	7.32	46.60	4.51
	negative direction	−129.41	−6.63	−47.70	6.61
0.4	forward	137.52	6.91	48.96	4.17
	negative direction	−135.00	−6.91	−45.49	4.51
0.5	forward	154.41	6.48	47.12	3.90
	negative direction	142.49	5.43	−48.51	5.23
0.6	forward	162.86	6.70	43.59	3.63
	negative direction	150.63	6.01	−46.90	4.08
0.7	forward	184.38	6.86	48.71	3.11
	negative direction	176.80	5.92	−48.31	3.31
0.8	negative direction	173.84	6.34	46.34	2.88
	negative direction	135.99	7.32	−46.64	3.69

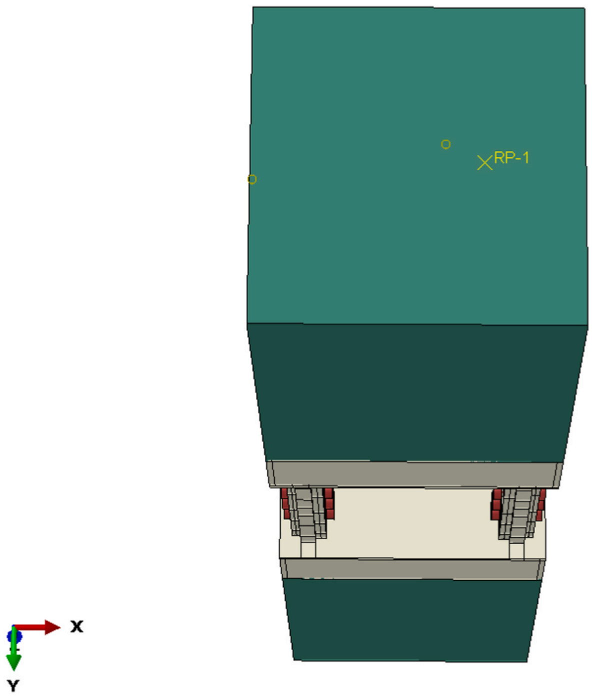

Fig. 17. Effect of eccentricity.

4.2. *Effect of eccentricity*

Four eccentric distances 25 mm, 50 mm, 75 mm, and 100 mm are selected to study the effect of eccentricity (Fig. 17). The comparisons the hysteresis curves and skeleton curves are shown in Figs. 18 and 19. The overall trend of the hysteresis curves of the joints with different eccentric distances is the same. With increase of the eccentricity, the bearing capacity of positive load decreases and the bearing capacity of negative load increases. This phenomenon is due to the fact that the eccentric distance of the joint is relative to the positive X-axis. The ultimate load capacity of the joint decreases with the increase of the eccentricity. All joints reach the ultimate load at a displacement of about 14 mm.

The energy dissipation capacity comparison is shown in Fig. 20. It indicts that the axial pressure ratio almost has no effect on the energy dissipation capacity. The ductility parameter is listed in Table 9. The ductility coefficient of the joint in the positive direction decreases with the increase of eccentricity while the ductility coefficient of the joint in the negative direction increases with the increase of eccentricity. The ductility coefficient in the positive direction is 3.91 when the eccentricity is 25 mm, and it is reduced by 64.7% to 1.38 when the eccentricity is 100 mm. It shows that the larger the eccentricity of the joint, the smaller the ductility coefficient in the positive direction and the larger the ductility coefficient in the negative direction.

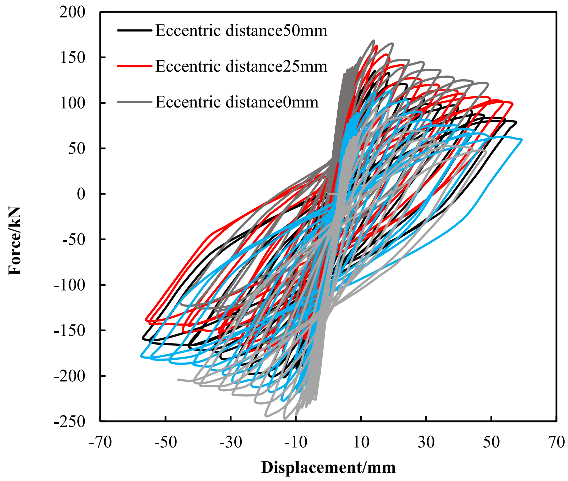

Fig. 18. Hysteresis curve comparison.

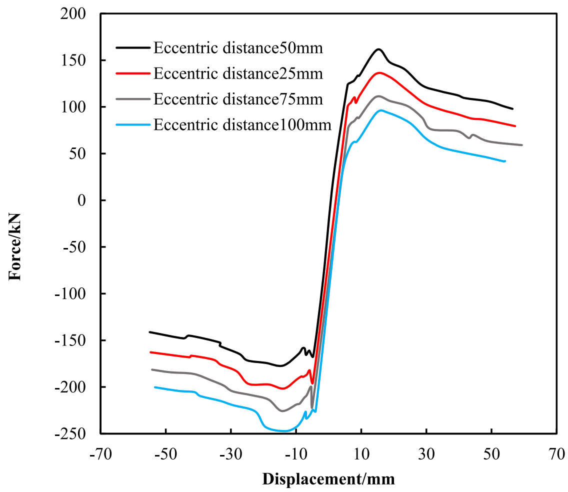

Fig. 19. Skeleton curve comparison.

5. Conclusion

A new type of detachable precast concrete column-column joint (DPC) is proposed in this study to solve the problems in current column-column dry connections. The dry connection technology is applied by composing of steel plate and concrete. The benchmark models are initially created and validated against the test data and after that a small-scale parametric study is organized. The effect of axial pressure ratio and eccentricity distance size on the seismic performance of DPC was studied. It is found that the DPC joint with axial pressure ratio of 0.7 has the best energy dissipation capacity and the joint with axial pressure ratio of 0.4 has the lowest energy dissipation capacity. With increase of the axial pressure ratio, the ductility coefficient shows a decreasing trend in general. The ductility coefficient of the joint in the positive direction decreases with the increase of eccentricity while the ductility coefficient of the joint in the negative direction increases with the increase of eccentricity.

Statements for conflicts of interest

The author of this paper with title of Structural performance of detachable precast concrete column-column joint receives research funding by the Scientific Research Start-up Funding of Shantou University (NTF22010) and Natural Science Foundation Funding of Guangdong Province (No. 2023A1515012502).

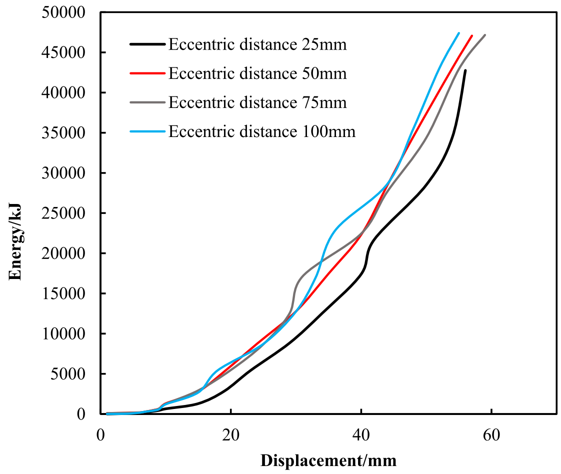

Fig. 20. The energy dissipation capacity comparison.

Table 9
The ductility parameter comparison.

models	Loading direction	yield point		Ultimate displacement (mm)	μ_u
		load capacity (kN)	displacement (vector) (mm)		
25 mm	forward	123.05	6.33	54.45	3.91
	negative direction	−164.10	−4.89	−54.91	7.34
50 mm	forward	111.28	9.17	57.25	2.76
	negative direction	−188.26	−5.36	−54.66	6.58
75 mm	forward	92.20	10.20	59.31	2.63
	negative direction	−205.47	−5.46	−54.19	6.77
100 mm	forward	59.55	27.86	54.16	1.38
	negative direction	−225.18	−4.75	−53.29	8.20

CRediT authorship contribution statement

H. Zhan: Investigation. **M. Ye:** Investigation, Data curation. **J. Jiang:** Supervision, Project administration, Methodology, Funding acquisition, Conceptualization. **C.W. Zheng:** Data curation. **S.C. Duan:** Data curation.

Declaration of competing interest

The authors declare the following financial interests/personal relationships which may be considered as potential competing interests:Jiang Jin reports financial support was provided by Natural Science Foundation Funding of Guangdong Province (No. 2023A1515012502). If there are other authors, they declare that they have no known competing financial interests or personal relationships that could have appeared to influence the work reported in this paper.

References

[1] National Development and Reform Commission, Ministry of Housing and Urban-Rural Development. Green building action program [EB/OL]. http://www.gov.cn/zwgk/2013-01/06/content_2305793.htm..
[2] General Office of the State Council. Guidance of the General Office of the State Council on vigorously developing assembly-type buildings [EB/OL]. http://www.gov.cn/zhengce/content/2016-09/30/content_5114118.htm..
[3] Kecai Du, Research on Mechanical Properties of I-Beam Connections in Reinforced Concrete Precast Beam-Column Members, Harbin Institute of Technology, 2017.
[4] Yuanqing Wang, Xueliang Qiao, Lianguang Jia, Tianxiong Zhang, Qinglin Jiang, Experimental study on the seismic performance of stainless steel beam-column nodes with different connection methods, J. Southeast Univ. (Nat. Sci. Ed.) 48 (2) (2018) 316–322.
[5] Zuozhou Zhao, Jian Zhou, Jianqun Hou, Baoshuang Ren, A review of horizontal joint shear mechanism and bearing capacity calculation methods for assembled concrete shear wall structures, Building Structure 45 (12) (2015) 39–47.
[6] Haishen Wang, M. Edoardo, Marino, Peng Pan, Design, Testing and Finite Element Analysis of an Improved Precast Prestressed Beam-To-Column Joint, Engineering Structures, 2019, p. 199.
[7] Weiming Yan, Wenming Wang, Shicai Chen, Hongquan Li, J. Gao, Experimental study on seismic performance of assembled precast concrete beam-column-stacked slab edge nodes, J. Civ. Eng. 43 (12) (2010) 56–61.

[8] Shicai Chen, Weiming Yan, Zhenbao Li, Wenming Wang, J. Gao, Experimental study on the overall seismic performance of nodes in large precast concrete beam-column laminated slabs, Eng. Mech. 29 (2) (2012) 135–141.
[9] T.M. Sheikh, G.G. Deierlein, J.A. Yura, et al., Beam-column moment connections for composite frames: part 2, J. Struct. Eng. 115 (11) (2016) 2858–2876.
[10] Jianjiang Yang, Hao Zhijun, Experimental study on the force performance of steel beam-reinforced concrete column nodes under low circumferential repeated loads, Building Structures (7) (2001) 35–38+42.
[11] Caihua Shi, Experimental Study of Assembled Concrete Beam-Column Nodes with Steel Plate Bolted Connections, Beijing University of Architecture, 2017.
[12] Ju-Yun Hu, Won-Kee Hong, Seon-Chee Park, Experimental investigation of precast concrete based dry mechanical column-column joints for precast concrete frames, Struct. Des. Tall Special Build. 26 (5) (2017) n/a-n/a.
[13] Ryo Yamashita, H.S. David, Ers. Seismic performance of precast Unbonded prestressed concrete columns, Structural Journal 106 (6) (2009).
[14] Gang Shi, Hao Yin, Fangxin Hu, Experimental study on seismic behavior of full-scale fully prefabricated steel frame: global response and composite action, Eng. Struct. 169 (2018).
[15] Sudhakar A. Kulkarni, Bing Li, Woon Kwong Yip, Finite element analysis of precast hybrid-steel concrete connections under cyclic loading, Journal of Constructional Steel Research 64 (2) (2007).
[16] Z. Jiang, X. Yang, C. Dou, et al., Seismic performance of prefabricated Corrugated web beam-column joint with replaceable cover plates, Adv. Struct. Eng. 22 (5) (2019) 1161–1174.
[17] J.D. Nzabonimpa, W.K. Hong, Experimental and nonlinear numerical analysis of precast concrete column splices with high-yield metal plates, Journal of structural engineering 145 (2) (2019), 04018254.1-04018254.15.
[18] J.D. Nzabonimpa, W.K. Hong, Structural performance of detachable precast composite column joints with mechanical metal plates, Eng. Struct. 160 (2018) 366–382.
[19] J.D. Nzabonimpa, W.K. Hong, J. Kim, Mechanical connections of the precast concrete columns with detachable metal plates, Struct. Des. Tall Special Build. 26 (17) (2017) e1391.
[20] J.D. Nzabonimpa, W.K. Hong, J. Kim, Nonlinear finite element model for the novel mechanical beam-column joints of precast concrete-based frames, Comput. Struct. 189 (2017) 31–48.
[21] J.D. Nzabonimpa, W.K. Hong, Experimental investigation of hybrid mechanical joints for L-shaped columns replacing conventional grouted sleeve connections, Eng. Struct. 185 (2019) 243–277.
[22] J.D. Nzabonimpa, W.K. Hong, J. Kim, Experimental and Non-linear Numerical Investigation of the Novel Detachable Mechanical Joints with Laminated Plates for Composite Precast Beam-Column Joint, Composite Structures, 2018. S026382231733461X.
[23] Wei Biyang, Research on the Seismic Performance of New Assembled Monolithic columns[D], Xi'an University of Architecture and Technology, 2014.
[24] D.F. Zhang, H. Gan, Finite element analysis of multi-groove assembled column connection nodes, J. Changchun Univ. Technol. (Nat. Sci. Ed.) 41 (3) (2018) 46–49+59.
[25] Hua Huang, Ming Li, Yujie Yuan, Hao Bai, Experimental research on the seismic performance of precast concrete frame with replaceable artificial controllable plastic hinges. (ASCE), J. Struct. Eng. 149 (1) (2023) 04022222.
[26] Hua Huang, Ming Li, Yujie Yuan, Hao Bai, Theoretical analysis on the lateral drift of precast concrete frame with replaceable artificial controllable plastic hinges, J. Build. Eng. 62 (2022) 105386.
[27] Hua Huang, Ming Li, Wei Zhang, Yujie Yuan, Seismic behavior of a friction-type artificial plastic hinge for the precast beam-column connection, Arch. Civ. Mech. Eng. (22) (2022) 201.
[28] M. Alhassan, R.Z. Al-Rousan, L.K. Amaireh, M.H. Barfed, Nonlinear finite element analysis of BC connections: influence of the column axial load, jacket thickness, and fiber dosage, Structures 16 (2018, November) 50–62. Elsevier.
[29] R.Z. Al-Rousan, M.A. Alhassan, R.J. Al-omary, Response of interior beam-column connections integrated with various schemes of CFRP composites, Case Stud. Constr. Mater. 14 (2021) e00488.
[30] R.Z. Al-Rousan, A. Sharma, Integration of FRP sheet as internal reinforcement in reinforced concrete beam-column joints exposed to sulfate damaged, Structures 31 (2021, June) 891–908. Elsevier.
[31] Jin Jiang, Z.S. Dai, Y.B. Wang, M. Ye, Experimental study on fracture toughness of quenched and tempered and TMCP high strength steels, Journal of Constructional Steel Research 189 (2022) 107096.
[32] Jin Jiang, Z.Y. Peng, W. Bao and M. Ye. Thermal effect of welding on mechanical behaviour of TMCP high strength steel, J. Mater. Civ. Eng., Volume 32 Issue 2, 04019364..
[33] Jin Jiang, Z.Y. Peng, Z.J. Ye, M. Ye, Behaviour of 690 MPa high strength steel built-up H-section columns under eccentric load scenarios, Eng. Struct. 213 (2020) 110550.
[34] Jin Jiang, Z.J. Ye, W. Bao, Y.B. Wang, X. Wang, X.H. Dai, Flexural buckling behaviour of 690 MPa high strength steel H-section columns, Eng. Struct. 200 (2019) 109718.
[35] Jin Jiang, S.P. Chiew, C.K. Lee and P.L.Y. Tiong. Numerical investigation of high strength built-up box column, Proceedings of the Institution of Civil Engineers-Structures and Buildings..
[36] Fei Gao, Zhiqiang Tang, Biao Hu, Junbo Chen, Hongping Zhu, Jian Ma, Investigation of the interior RC beam-column joints under monotonic antisymmetrical load, Front. Struct. Civ. Eng. 13 (2019) pages1474–1494.
[37] Hao Fu, Design and Research of New Prefabricated Loading Beam-Column Nodes [D], Guangzhou University, 2019.
[38] Southeast University, Concrete Structures . Upper Volume, Principles of Concrete Structure Design, China Construction Industry Press, 2008.
[39] X.R. Li, B. Qin, Handbook of Steel Structure Connection Node Design, fourth ed., China Construction Industry Press, 2019.
[40] J.H. Li, F. Wang, D.L. Qiu, et al., Study on the shear force transfer performance of steel-concrete sections with pinned joints, J. Civ. Eng. 45 (12) (2012) 74–82.
[41] The national standard of steel structure design gb50017-2017, China Building Metal Structure (2) (2018) 72.
[42] J. Lee, G.L. Fenves, A plastic-damage concrete model for earthquake analysis of dams, Earthquake engineering & structural dynamics 27 (9) (1998) 937–956.
[43] C. Zhang, D. An, L. Zhu, Axial compressive behavior of steel-damping-concrete composite wall, Appl. Sci. 9 (21) (2019) 4679.
[44] M. Ye, J. Jiang, H.M. Chen, H.Y. Zhou, D.D. Song, Seismic behavior of an innovative hybrid beam-column connection for precast concrete structures, Eng. Struct. 227 (2021) 111436.
[45] J. Jiang, M. Wu, M. Ye, Prediction of Fire Spalling Behaviour of Fibre-Reinforced Concrete, Magazine of Concrete Research, 2023, pp. 1–16.
[46] J. Jiang, M. Ye, L.Y. Chen, Z.W. Zhu, M. Wu, Study on static strength of Q690 built-up K-joints under axial loads, Structures 51 (2023) 760–775.